Asian Journal of Pharmaceutical Sciences 18 (2023) 100846

Available online at www.sciencedirect.com

ScienceDirect

journal homepage: www.elsevier.com/locate/AJPS

Original Research Paper

# Nano transdermal system combining mitochondria-targeting cerium oxide nanoparticles with all-trans retinoic acid for psoriasis

*Wei Wang*[a,1], *Xinyi Xu*[b,1], *Yanling Song*[b], *Lan Lan*[c], *Jun Wang*[a], *Xinchang Xu*[a,*], *Yongzhong Du*[b,d,*]

[a] *Department of Pharmacy, Hangzhou Third People' s Hospital, Affiliated Hangzhou Dermatology Hospital, Zhejiang University School of Medicine, Hangzhou 310009, China*

[b] *College of Pharmaceutical Sciences, Zhejiang University, Hangzhou 310058, China*

[c] *Department of Dermatology, Affiliated Hangzhou Dermatology Hospital, Zhejiang University School of Medicine, Hangzhou 310009, China*

[d] *Innovation Center of Translational Pharmacy, Jinhua Institute of Zhejiang University, Jinhua 321299, China*

ARTICLE INFO

*Article history:*
Received 19 May 2023
Revised 16 August 2023
Accepted 1 September 2023
Available online 24 September 2023

*Keywords:*
Psoriasis
Cerium oxide nanoparticles
All-trans retinoic acid
Flexible nanoliposomes
Transdermal delivery

ABSTRACT

Psoriasis is an inflammatory skin disease that is intricately linked to oxidative stress. Antioxidation and inhibition of abnormal proliferation of keratinocytes are pivotal strategies for psoriasis. Delivering drugs with these effects to the site of skin lesions is a challenge that needs to be solved. Herein, we reported a nanotransdermal delivery system composed of all-trans retinoic acid (TRA), triphenylphosphine (TPP)-modified cerium oxide ($CeO_2$) nanoparticles, flexible nanoliposomes and gels ($TCeO_2$-TRA-FNL-Gel). The results revealed that $TCeO_2$ synthesized by the anti-micelle method, with a size of approximately 5 nm, possessed excellent mitochondrial targeting ability and valence conversion capability related to scavenging reactive oxygen species (ROS). $TCeO_2$-TRA-FNL prepared by the film dispersion method, with a size of approximately 70 nm, showed high drug encapsulation efficiency (>96%). $TCeO_2$-TRA-FNL-Gel further showed sustained drug release behaviors, great transdermal permeation ability, and greater skin retention than the free TRA. The results of *in vitro* EGF-induced and $H_2O_2$-induced models suggested that $TCeO_2$-TRA-FNL effectively reduced the level of inflammation and alleviated oxidative stress in HaCat cells. The results of *in vivo* imiquimod (IMQ)-induced model indicated that $TCeO_2$-TRA-FNL-Gel could greatly alleviate the psoriasis symptoms. In summary, the transdermal drug delivery system designed in this study has shown excellent therapeutic effects on psoriasis and is prospective for the safe and accurate therapy of psoriasis.



* Corresponding authors.
*E-mail addresses:* zxyyadr@163.com (X. Xu), duyongzhong@zju.edu.cn (Y. Du).

[1] These authors contributed equally to this work.

Peer review under responsibility of Shenyang Pharmaceutical University.

https://doi.org/10.1016/j.ajps.2023.100846

## 1. Introduction

Psoriasis is an inflammatory skin disease mainly mediated by immunity and it affects millions of people around the world [1–2]. It is reported that topical therapy, phototherapy, and immunotherapy have been used for the treatment [3–5]. Topical therapy mainly utilizes drugs such as retinoids, vitamin D derivatives to treat psoriasis [6]. These drugs are effective to some extent, but their demerits, including skin irritation and instability, are still stumbling blocks for better clinical efficacy [7]. Hence, the exploration of an appropriate drug delivery system is of vital necessity and urgency for patients.

Retinoic acid has been used to treat skin disease for nearly 40 years [8]. All-trans retinoic acid (TRA) is regarded as the first-generation therapeutic drug used for skin diseases, such as wound healing, acne, and psoriasis [9–11]. TRA can bind with retinoic acid receptors such as RAR-α and RAR-$\gamma$ and then regulate the abnormal differentiation of keratinocytes, which is beneficial for relieving the proliferation of keratinocytes and reducing the level of inflammation [12,13]. Although TRA is useful for psoriasis, its application is hindered because of its sensitivity to light and oxygen, poor water solubility, and skin irritation [14].

In addition to conventional therapy, the mitigation of oxidative stress is also important for psoriasis [15]. When the skin is exposed to oxidative stress, a large amount of reactive oxygen species (ROS) is generated that can participate in promoting cell proliferation, differentiation, and inflammation by regulating signal pathways such as NF-$\kappa$B, MAPK and JAK-STAT pathways [16]. Natural compounds such as epigallocatechin-3-gallate, glycyrrhizic isoflavones and proanthocyanidins have been used to alleviate the oxidative stress state of psoriasis [17–19]. However, the use of these active components is still limited because their efficient extraction and separation still need further study. Recently, nanomaterials with enzyme-like activity have attracted research interest. Among nanomaterial-based antioxidants, cerium oxide ($CeO_2$) nanoparticles exhibit tremendous potential as superoxide dismutase (SOD)/catalase (CAT)-mimetics by scavenging ROS through shuttling between the redox state ($Ce^{3+}$) and oxidation state ($Ce^{4+}$) [20,21]. They have also been applied in major diseases, including Alzheimer's disease, ischemic stroke, and cancer [22–24]. The activity of eradicating ROS makes $CeO_2$ a promising candidate for psoriasis therapy. Meanwhile, there is a close connection between mitochondria and ROS. Both endogenous and exogenous ROS can easily damage mitochondrial DNA (mtDNA) because mtDNA has the limited repair capacity and a lack of histone barrier [25,26]. mtDNA damage causes mitochondrial dysfunction and is mainly involved in psoriasis through two pathways. On the one hand, mtDNA is released into the cytoplasm as mitochondrial damage-associated molecular patterns, activating Toll-like receptor (TLR)−9[27,28]. The activation of TLR-9 can take part in subsequent inflammatory processes by inducing several signaling pathways [29–31]. On the other hand, mtDNA damage can lead to loss of mitochondrial polypeptide expression to cause defective functioning of the electron transport chain (ETC), further increasing ROS [32–34]. ROS can participate in promoting cell proliferation, differentiation, and inflammation by regulating some signaling pathways [16]. Hence, a mitochondria-targeting strategy is beneficial for psoriasis therapy. Triphenylphosphine (TPP) is a lipophilic cation whose lipid solubility and positive charge endow it with mitochondria-targeting ability [35,36]. The combination of $CeO_2$ and TPP can anchor the mitochondria of keratinocytes and accurately remove ROS. However, the poor skin absorption of $CeO_2$ is the main obstacle remaining to be solved.

Transdermal delivery is attractive for the treatment of psoriasis because of the imperfect skin barrier, but it is challenging to realize efficient and safe delivery [37]. On the one hand, the stratum corneum can extremely block the penetration of most drugs due to its highly organized structure [38]. On the other hand, some properties, such as high molecular weight and poor water solubility, affect drug delivery [39]. In particular, the broken barrier also limits the delivery of drugs with skin irradiation in some skin diseases, such as psoriasis. Currently, many novel drug delivery systems have been explored such as dendrimers, ethosomes and transfersomes [40–42]. Flexible nanoliposomes are prospective carriers for transdermal delivery. It can increase the stability of encapsulated drugs and increase the permeability of drugs into the skin [43]. Distinct from the rigid structure of liposomes, they contain membrane softeners such as ethanol, Tween-80, and cholate, which contribute substantially to their high deformability, flexibility, and skin permeability [44,45]. Flexible nanoliposomes are commonly used in skin diseases, such as wound healing and psoriasis. Topical gels aiming to realize the efficient delivery of drugs to skin are also used in skin diseases to improve skin adhesion and prolong skin retention time [45].

In particular, we reported a nanotransdermal delivery system composed of TRA, TPP-modified $CeO_2$ nanoparticles, flexible nanoliposomes, and gels ($TCeO_2$-TRA-FNL-Gel). TRA inhibited the excessive proliferation of keratinocytes, and $TCeO_2$ effectively scavenged ROS by targeting mitochondria, thus alleviating oxidative stress in psoriatic skin. Using flexible nanoliposomes as carriers could improve drug stability and penetration efficiency by virtue of their high deformability and excellent permeability as well as significantly increase drug accumulation in the dermis. The uniform and stable network structure of gels could improve the adhesion of flexible nanoliposomes to skin and finally achieve the safe and accurate treatment of psoriasis.

## 2. Materials and methods

### 2.1. Materials

Cerium (III) acetate hydrate, soybean lecithin, TRA and carbomer 940 were obtained from Dalian Meilun Biotechnology Co., Ltd. (Dalian, China). Oleylamine, xylene, triphenylphosphine and Tween-80 were obtained from Macklin Biochemical Co., Ltd. (Shanghai, China). Fluorescein isothiocyanate was obtained from Aladdin Biochemical Technology Co., Ltd. (Shanghai, China). Fetal bovine serum

(FBS) was obtained from Hangzhou Tianhang Biotechnology Co., Ltd. (Hangzhou, China). Dulbecco's minimum essential medium (DMEM) was obtained from Senrui Biotechnology Co., Ltd. (Zhejiang, China). IMQ (5%) was obtained from Sichuan Med-shine Pharmaceutical Co., Ltd. (Sichuan, China). ELISA kits for IL-6 and TNF-$\alpha$ were obtained from Jiangsu Meimian Industrial Co., Ltd. (Jiangsu, China). SOD kits and ROS kits were obtained from Beyotime Biotechnology Co., Ltd. (Shanghai, China). HaCat cells were obtained from Procell Life Science & Technology Co., Ltd. (Wuhan, China) and cultured in DMEM with 10% FBS in a 37 °C cell incubator with 5% $CO_2$. BALB/c mice (female, 6 weeks old, 15 to 20 g) were obtained from Hangzhou Medical College (Hangzhou, China). All animal experiments were conducted according to the rules of the animal care and use committee of Zhejiang University.

### 2.2. Synthesis of $TCeO_2$

TPP-modified $CeO_2$ ($TCeO_2$) nanoparticles were synthesized by the reverse micelle method [46,47]. A total of 0.43 g cerium (III) acetate hydrate, 2.14 g oleylamine, and 1.05 g TPP were added into 15 ml xylene and then heated at 90 °C under an argon atmosphere after stirring for 18 h. When the liquid became clear, 1 ml deionized water was quickly added, then continuously heated at 90 °C for 3 h until the liquid turned yellow. After cooling to room temperature, 100 ml ethanol and centrifugation (4,000 rpm, 15 min) were used to collect $TCeO_2$, which was finally stored in chloroform.

### 2.3. Characterization of $TCeO_2$

The particle size and morphology were observed by dynamic light scattering (DLS) instrument (Litesizer 500, Anton-Paar, Austria) and transmission electron microscopy (TEM) (JEM-1400, JEOL, Japan). Spectra of samples were analyzed by Fourier transform infrared spectrometry (FTIR) (NICOLET iS50FT-IR, Thermo Scientific, USA) and nuclear magnetic resonance spectroscopy (NMR) (Avance III 500 M, Bruker Biospin, Switzerland). The cerium ion valence was obtained by X-ray photoelectron spectroscopy (XPS) (ESCALAB 250Xi, Thermo Scientific, USA), and the valence cycling ability was evaluated by stimulating $H_2O_2$. The cerium concentration was analyzed by inductively coupled plasma–optical emission spectrometry (ICP-MS) (Agilent 7800, Agilent Technologies, USA).

### 2.4. Preparation and characterization of flexible nanoliposomes

Flexible nanoliposomes coloaded with $TCeO_2$ and TRA ($TCeO_2$-TRA-FNL) were obtained by film dispersion method. First, soybean lecithin, Tween 80, TRA and $TCeO_2$ were added into 10 ml absolute ethanol according to Table 1. Second, the mixture was evaporated in the dark until the film was completely formed, and then PBS (4 ml, pH 6.8) was added for hydration. Finally, $TCeO_2$-TRA-FNL was obtained after probe sonication.

The particle size and morphology were observed by DLS and TEM. Encapsulation efficiency (EE) and drug loading (DL) were measured by ultrafiltration centrifugation. In brief, 0.5 ml flexible nanoliposome suspension was ultrafiltered (MWCO: 100 kD) and centrifuged (5,000 rpm, 10 min) to separate the free and encapsulated TRA. The concentrations of TRA were detected by HPLC shown in Table S1. The concentrations of unencapsulated cerium and total cerium were detected by ICP–MS. The following equations were used to calculate the EE and DL:

**Table 1 – Weight of added substances in liposomes.**

| Substance | Added weight (mg) |
|---|---|
| Soybean lecithin | 400 |
| Tween 80 | 80 |
| TRA | 4 |
| Cerium in $TCeO_2$ | 4 |

$$\text{EE}\ (\%) = \frac{\text{total mass of drug} - \text{mass of unencapsulated drug}}{\text{total mass of drug}} \times 100\%$$

$$\text{DL}\ (\%) = \frac{\text{total mass of drug} - \text{mass of unencapsulated drug}}{\text{total mass of liposomes}} \times 100\%$$

### 2.5. Preparation of gel loaded with flexible nanoliposomes

The blank gel was first prepared according to the prescription, in which carbomer 940, glycerin, EDTA and ethylparaben accounted for 1%, 10%, 0.1%, 0.1% (w/w), respectively. Next, the pH was adjusted to 6.5 by adding triethanolamine. Finally, the nanoliposomes were mixed with blank gel, and the TRA content was controlled to 0.05% to obtain the final gel.

### 2.6. In vitro TRA release of gel

The TRA release behavior of the gel was investigated by the dialysis method, and a mixture of ethanol and PBS (pH 6.8) (1:1, v/v) was used as the release medium. Next, 0.5 g of the gel was added into a dialysis bag (MWCO: 3.5 kD) and then put in 10 ml release medium with sustained oscillation (60 rpm, 37 °C). The whole release medium was collected at preset time points and TRA concentration was determined by HPLC.

### 2.7. In vitro skin retention and permeability of gel

The skin retention and permeability of gel was investigated by the diffusion cell method with skin obtained from an experimental pig. A mixture of ethanol and PBS (pH 6.8) (1:1, v/v) was the receiving medium. The skin was fixed flat on the junction of the diffusion cell. 1 g of gel was put into the donor chamber and 15 ml the medium was added into the receptor chamber (37 °C, 300 rpm). Then, 200 µl the receiving medium was collected at preset time points and TRA concentration was determined by HPLC.

Next, the skin was collected and cleaned with PBS (pH 6.8), and TRA was extracted with 1 ml methanol. The TRA concentration that remained in the skin was determined by HPLC after centrifugation (5,000 rpm, 10 min). Skin treated with FITC-labeled $TCeO_2$-TRA-FNL-Gel for 24 h was also taken as the sample to evaluate the time-dependent skin permeability.

### 2.8. Rheology characterization of gel

The kinetics of gel were studied by a rheometer (DHR 2, TA instrument, America). Gels with a thickness of 1 mm were placed between the parallel plate (25 mm in diameter) and the rheometer. A strain sweep test was performed from 0.01% to 1,000% (frequency: 1 Hz) to measure the modulus of the gels (G': storage modulus, G'': loss modulus) [48]. The complex viscosity of gels was also obtained in this process.

### 2.9. In vitro cytotoxicity

HaCat cells were incubated for 24 h ($1 \times 10^4$ cells/well, 96-well plates). $TCeO_2$-TRA-FNL (0, 250, 500, 750, 1,000, 1,250, 1,500 and 2,000 μg/ml) was added and then cultured for 24 h. Every concentration had six repetitions. The viability of HaCat cells was studied by CCK-8 assay.

### 2.10. Cellular uptake

HaCat cells were incubated for 24 h ($5 \times 10^4$ cells/well, 24-well plates). FITC-labeled $TCeO_2$-TRA-FNL (400 μg/ml) was added and then cultured for preset time points. The process of cellular uptake was observed through confocal laser scanning microscopy (CLSM).

### 2.11. Mitochondria-targeting ability

First, ODA-FITC and $TCeO_2/CeO_2$ were mixed (1:2, w/w) and stirred continuously for 8 h to obtain FITC-labeled $TCeO_2/CeO_2$. Then, FITC-labeled $TCeO_2$-FNL/$CeO_2$-FNL was prepared following the method mentioned previously.

HaCat cells were incubated for 24 h ($5 \times 10^4$ cells/well, 24-well plates). FITC-labeled $TCeO_2$-FNL/$CeO_2$-FNL (400 μg/ml) was added and then cultured for preset time points. Finally, MitoTracker Deep Red (100 nM) was coincubated with HaCat cells for 40 min to stain the mitochondria. The colocalization between $TCeO_2$-FNL/$CeO_2$-FNL and mitochondria was observed through CLSM and ImageJ.

### 2.12. In vitro antioxidant ability

*Intracellular ROS detection:* HaCat cells were incubated for 24 h ($1 \times 10^5$ cells/well, 12-well plates). After preincubation with different preparations ($TCeO_2$-TRA-FNL, $TCeO_2$-FNL, $CeO_2$-FNL, TRA-FNL, and Free-TRA) for 4 h, HaCat cells were treated with $H_2O_2$ (750 μM) for 24 h. Then, a DCFH-DA probe (10 μM) was coincubated with HaCat cells for 30 min. Finally, the ROS detection were observed through CLSM.

*SOD level determination:* HaCat cells were incubated for 24 h ($1 \times 10^5$ cells/well, 12-well plates). After preincubation with different preparations ($TCeO_2$-TRA-FNL, $TCeO_2$-FNL, $CeO_2$-FNL, TRA-FNL, and Free-TRA) for 4 h, HaCat cells were treated with $H_2O_2$ (750 μM) for 24 h. Then, the supernatant collected by lysis and centrifugation (12,000 rpm, 10 min) was used to determine the level of SOD.

### 2.13. In vitro anti-inflammatory ability

HaCat cells were incubated for 24 h ($1 \times 10^5$ cells/well, 12-well plates). After preincubation with EGF (80 ng/ml) for 1 h, HaCat cells were treated with different preparations ($TCeO_2$-TRA-FNL, $TCeO_2$-FNL, $CeO_2$-FNL, TRA-FNL, and Free-TRA) for 24 h. Then, the supernatant after centrifugation (12,000 rpm, 10 min) was collected to determine the level of interleukin-6 (IL-6)/tumor necrosis factor–$\alpha$ (TNF–$\alpha$).

### 2.14. Establishment of the psoriasis model

The psoriasis model can be established by applying 5% IMQ at a daily dosage of 62.5 mg to the depilated back skin(2 cm×1.5 cm) for 7 d.

### 2.15. Psoriasis treatment

BALB/c mice were randomly divided into seven groups: (1) control group, (2) IMQ group, (3) $TCeO_2$-TRA-FNL-Gel group, (4) $TCeO_2$-FNL-Gel group, (5) $CeO_2$-FNL-Gel group, (6) TRA-FNL-Gel group, and (7) Free-TRA-Gel group (for each group, $n = 5$). From Day 3, gels were applied at a daily dosage of 100 mg. The whole process, including model establishment and treatment, lasted for 7 d.

### 2.16. Weight observation and skin PASI score

The weight of the mice was recorded, and the skin condition was evaluated according to the psoriasis area and severity index (PASI).

### 2.17. Skin compliance study

A skin compliance study of gel was conducted on the skin of mice [49,50]. Gels were applied on the skin at 100 mg/d for 7 d The skin condition was recorded in the treatment (1, 3, 7, 10 d).

### 2.18. In vivo antioxidant ability

*ROS detection in diseased skin:* The skin tissue was stained with ROS dye, and the expression of ROS was detected by immunofluorescence. SOD level determination: PBS was utilized to grind the skin tissue into 10% homogenate. Then, centrifugation (12,000 rpm, 10 min) was used to collect the supernatant, which was utilized to determine the level of SOD.

### 2.19. In vitro anti-inflammatory ability

PBS was utilized to grind the skin tissue into a 10% homogenate. Then, centrifugation (12,000 rpm, 10 min) was used to collect the supernatant, which was utilized to measure the levels of IL-6/TNF-$\alpha$.

### 2.20. Skin histopathology and immunohistochemistry

The skin tissue was removed from back for H&E staining. At the same time, the expression levels of CD3, CD31 and Ki67 were examined by immunohistochemistry.

### 2.21. Statistical analysis

We utilize T test to determine differences between two groups. $P < 0.05$ was considered significant.

## 3. Results and discussion

### 3.1. Synthesis and characterization of $TCeO_2$

$TCeO_2$ was obtained by the reverse micelle method [46,47]. The DLS and TEM results were shown in Fig. 1A and 1B and Table S2. The particle size of $TCeO_2$ was 5.82 ± 0.24 nm, while that of $CeO_2$ was 4.54 ± 0.39 nm. Clearly, the sizes of both particles were small, and the TEM image also showed a small size and fine morphology. It has been reported that the ratio of surface area to volume was high due to the small size, which is beneficial for providing a large surface area for catalysis [51]. Hence, the $TCeO_2$ we synthesized might have potential catalytic activity.

The FTIR result in Fig. 1C showed that compared with $CeO_2$, new peaks (1120–1050 $cm^{-1}$) appeared in the spectrum of $TCeO_2$, which was consistent with that in the spectrum of TPP, indicating that TPP was successfully modified. The XPS analysis in Fig. 1D proved the existence of phosphorus, and the $^1H/^{13}C$ NMR results in Figs. 1F and S2 also implied that the same absorption belonging to the phenyl ring of TPP existed in TPP and $TCeO_2$. All the results further verified the modification of TPP, which is rational to target mitochondria for ROS elimination since TPP has been used to enhance the antioxidant ability of mitochondria in some studies [52,53]. In addition, utilizing the SOD/CAT-mimetic activity of $TCeO_2$ (SOD: $Ce^{3+}$, CAT: $Ce^{4+}$) to remove ROS has been reported to be reasonable and effective. Hence, the valence conversion of $TCeO_2$ also needs to be considered. Fig. 1E likewise showed that both $Ce^{3+}$ and $Ce^{4+}$ existed on the surface of $TCeO_2$ ($Ce^{3+}$: $u_1$, $v_1$; $Ce^{4+}$: $u_0$, $u_2$, $u_3$, $v_0$, $v_2$, $v_3$), which was of vital significance for the redox ability of $TCeO_2$. In addition, we could directly see the color cycling of the $TCeO_2$ dispersion within 20 d in Fig. 1G. When $Ce^{3+}$ was oxidized to $Ce^{4+}$ by $H_2O_2$, the color turned orange, while when $Ce^{4+}$ was converted to $Ce^{3+}$, the color gradually faded back to light yellow. The results both illustrated that $TCeO_2$ had excellent valence conversion ability and was the basis for ROS eradication, thus playing a prominent role in improving the antioxidant ability of mitochondria.

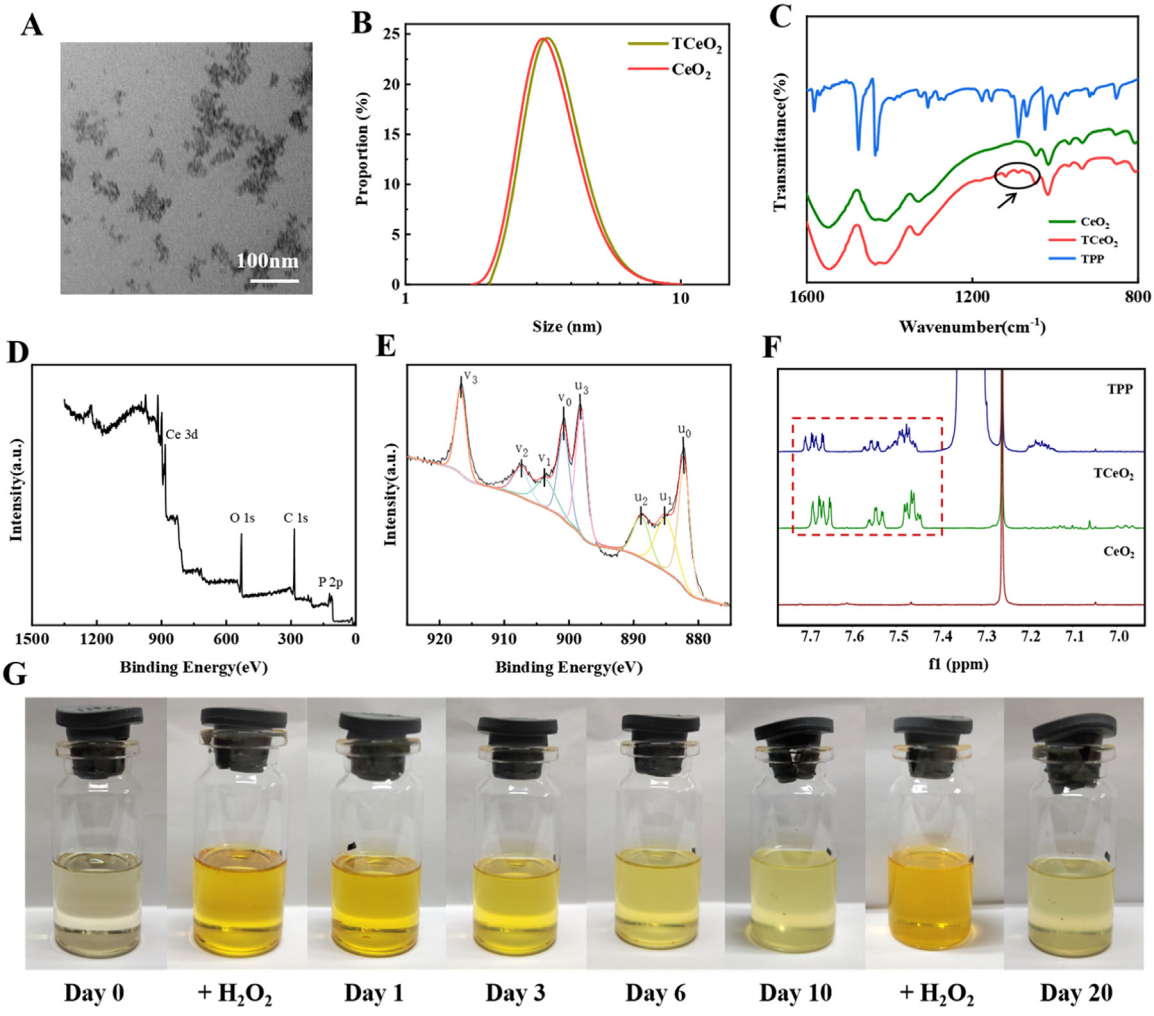


**Fig. 1 – Characterization of $TCeO_2$. (A-B) TEM image of $TCeO_2$, DLS results of $TCeO_2$ and $CeO_2$; (C) Infrared spectra of $CeO_2$, $TCeO_2$ and TPP; (D) XPS spectrum of $TCeO_2$; (E) Ce 3d XPS spectrum of $TCeO_2$ ($u_0$=882.20 eV, $u_1$=885.03 eV, $u_2$=888.78 eV, $u_3$=898.11 eV; $v_0$=900.80 eV, $v_1$=903.63 eV, $v_2$=907.38 eV, $v_3$=916.71 eV); (F) $^1H$ NMR spectra of TPP, $TCeO_2$, and $CeO_2$ (in $CDCl_3$); (G) The valence cycling ability of $TCeO_2$.**

### 3.2. *Preparation and characterization of gel loaded with flexible nanoliposomes*

The nanotransdermal delivery system we reported contained flexible nanoliposomes and gels. Therefore, flexible nanoliposomes and gels were prepared and then evaluated. We first determined the viability of HaCat cells treated with TRA (0–40 μg/ml) and cerium (0–60 μg/ml) for 24 h. As was shown in Fig. 2A and 2B, we ultimately chose the appropriate ratio of TRA to cerium (w/w, 1:1) to prepare flexible nanoliposomes. Fig. 2D and Table S3 revealed that the average sizes of different flexible nanoliposomes were nearly 60–70 nm, which means that they were promising for transdermal delivery [54]. TEM observation results in Fig. 2C and S1 also indicated that the liposomes had an obvious phospholipid bilayer and were relatively uniform in size. The smaller sizes of flexible liposomes than conventional liposomes were mainly due to the incorporation of Tween 80, which could achieve higher curvature [55]. In addition, the high encapsulation efficiency (TRA>96%, cerium>99%) shown in Table S3 might also be attributed to the properties of Tween 80 as a surfactant and solubilizer [56].

Next, gels were prepared, and TRA release behavior as well as skin retention and permeability were studied. Fig. 2E clearly showed that the release rate of TRA was rapid and nearly all the TRA was released within 8 h in Free-TRA-Gel. In contrast, TRA displayed a slow sustained release for 72 h when encapsulated into liposomes. The sustained release due to the lipid bilayer was helpful in the treatment because more drugs could accumulate in therapeutic sites for durable therapy and side effects were reduced [57]. Fig. 2F described the retention results, and it could be seen that the drug skin retention of $TCeO_2$-TRA-FNL-Gel was higher than that of Free-TRA-Gel ($P < 0.01$). Specifically, $TCeO_2$-TRA-FNL-Gel and TRA-FNL-Gel were 1.81 and 1.45 times the drug skin retention of Free-TRA-Gel.

The kinetics of gels were studied by a rheometer (G': solid property, G'': liquid property) [48]. It was evident that G' and G'' values were relatively stable in the strain range from 0.01% to 1%, indicating the linear viscoelastic region of $TCeO_2$-TRA-FNL-Gel. Then, G' values decreased while G'' values increased until intersecting at a strain of approximately 167.8%, which represented the breakdown of the gel network (Fig. 2G). A similar phenomenon was observed in other gels (Fig. S3). The results exhibited the viscoelasticity behavior of the gels we prepared, which was consistent with what a previous study reported [58]. The result in Fig. 2H implied that the decreasing viscosity of the gels was related to the increasing strain, which might be because the internal network of the gels was gradually destroyed [59].

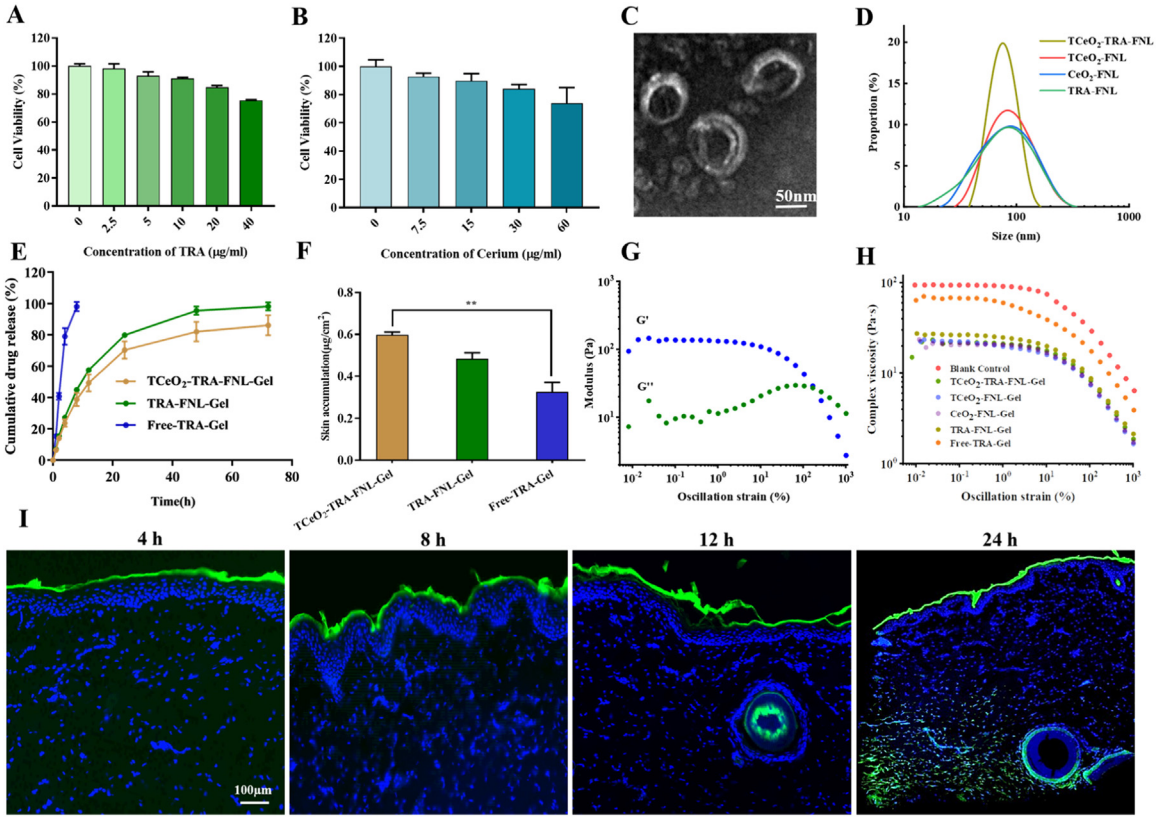


**Fig. 2 – Characterization of $TCeO_2$-TRA-FNL-Gel. (A-B) Viability of HaCat cells after treated with TRA (0–40 μg/ml)/Cerium (0–60 μg/ml) for 24 h; (C-D) TEM image of $TCeO_2$-TRA-FNL and DLS results of $TCeO_2$-TRA-FNL, $TCeO_2$-FNL, $CeO_2$-FNL and TRA-FNL; (E) *In vitro* TRA release behaviors of $TCeO_2$-TRA-FNL-Gel, TRA-FNL-Gel and Free-TRA-Gel; (F) *In vitro* skin retention of $TCeO_2$-TRA-FNL-Gel, TRA-FNL-Gel and Free-TRA-Gel; (G) The variation of G′ and G″ values with strain for $TCeO_2$-TRA-FNL-Gel; (H) The complex viscosity of gels; (I) CLSM images of pig skin after treatment with $TCeO_2$-TRA-FNL-Gel for preset time points. Data are expressed as the mean ± SD, $n = 3$, *$P < 0.05$, **$P < 0.01$, ***$P < 0.001$.**

Furthermore, from the skin permeation result shown in Fig. 2I, we found that the liposomes were mainly distributed on the surface of skin within 12 h due to the blocking effect of the stratum corneum. However, they penetrated downward into the dermis after 24 h, which might be attributed to the extended retention, prolonging the penetration time. The results above demonstrated the sustained release behavior and high skin retention and permeability of flexible nanoliposomes, which were beneficial to the treatment of local diseases such as psoriasis [60].

### 3.3. *Cytotoxicity and cellular uptake*

HaCat cells were treated with $TCeO_2$-TRA-FNL for 24 h and FITC-labeled $TCeO_2$-TRA-FNL for predetermined time points (2, 4, 8 and 12 h) to evaluate cytotoxicity and cellular uptake ability, respectively. As shown in Fig. 3A, $TCeO_2$-TRA-FNL (0–2000 μg/ml) showed no obvious cytotoxicity. We also observed that weak green fluorescence appeared after 2 h, and the fluorescence intensity gradually increased with the time of coincubation (Fig. 3B). In brief, $TCeO_2$-TRA-FNL prepared in this study had excellent biocompatibility and could be successfully absorbed by HaCat cells.

### 3.4. *Mitochondria-targeting ability*

The red probe for mitochondria was used to verify the mitochondria-targeting ability of $TCeO_2$. CLSM was used to observe fluorescence, and the results were shown in Fig. 3C and 3D. We observed that the fluorescence of $CeO_2$-FNL partially overlapped with that of mitochondria, and the possible reason might be the special properties of $CeO_2$, such as its small size and hydrophobicity [61]. Nonetheless, we found that the fluorescence overlap between $TCeO_2$-FNL and mitochondria was significantly higher. In addition, fluorescence semiquantitative analysis was obtained by ImageJ, and the results in Fig. 3E and 3F showed that the colocalization ratio between $TCeO_2$-FNL and mitochondria was higher than that of $CeO_2$-FNL, suggesting that $TCeO_2$-FNL had better mitochondria-targeting ability with the help of TPP.

### 3.5. *In vitro antioxidant and anti-inflammatory ability*

Inflammatory cytokines and oxidative stress-related factors are rich in psoriasis lesions; therefore, reducing the levels of these factors is critical for treating psoriasis [62,63].

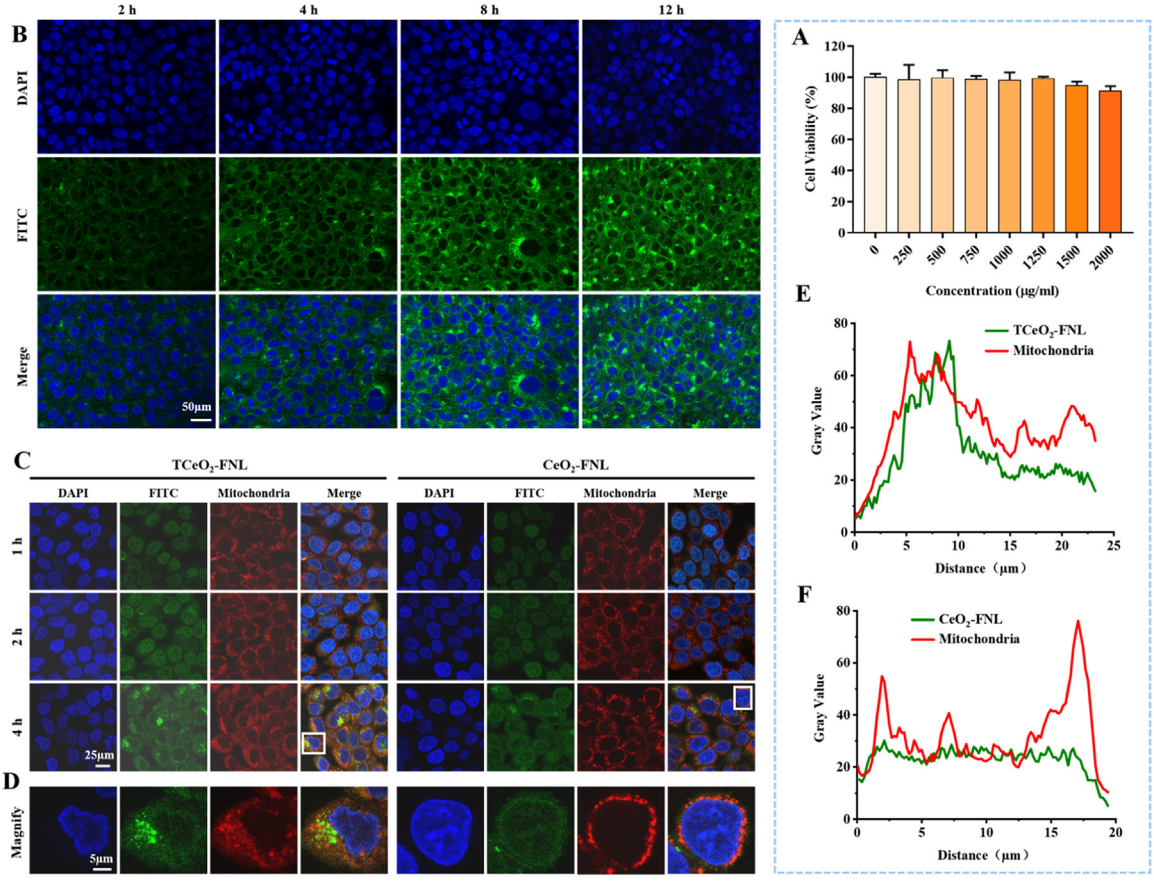


**Fig. 3 – Cytotoxicity and cellular uptake of $TCeO_2$-TRA-FNL and the mitochondria-targeting ability of $TCeO_2$-FNL/$CeO_2$-FNL. (A) Viability of HaCat cells after treatment with $TCeO_2$-TRA-FNL (0–2,000 μg/ml) for 24 h; (B) CLSM images of HaCat cells after treatment with $TCeO_2$-TRA-FNL for preset time points; (C-D) CLSM images of HaCat cells after treatment with $TCeO_2$-FNL/$CeO_2$-FNL for preset time points (red: mitochondria; green: $TCeO_2$-FNL/$CeO_2$-FNL); (E-F) Fluorescence intensity analysis of images from Fig. 3D, which shows the colocalization between $TCeO_2$-FNL/$CeO_2$-FNL and mitochondria. Data are expressed as the mean ± SD, $n = 3$, $^*P < 0.05$, $^{**}P < 0.01$, $^{***}P < 0.001$.**

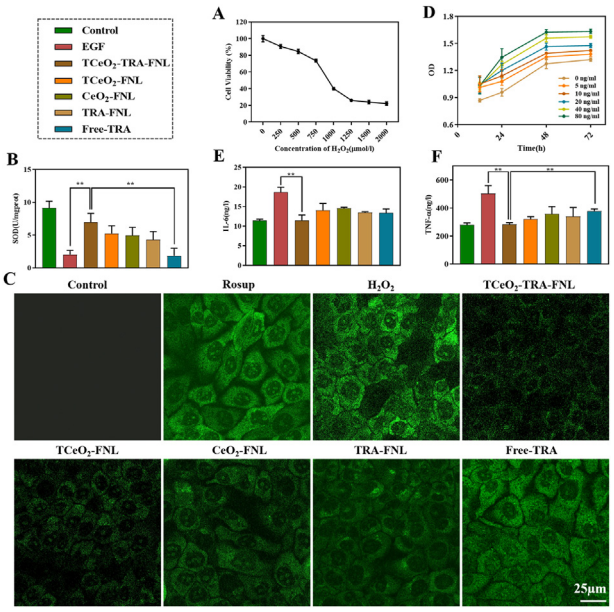


**Fig. 4 – *In vitro* antioxidant and anti-inflammatory ability of $TCeO_2$-TRA-FNL (the concentrations of TRA and cerium were both 10 μg/ml). (A) Cell viability of HaCat cells after incubation with $H_2O_2$ (0–2,000 μg/ml) for 24 h. (B) SOD activity of HaCat cells preincubated with different preparations for 4 h before treatment with $H_2O_2$ for 24 h. (C) Fluorescence images of HaCat cells preincubated with different preparations for 4 h before treatment with $H_2O_2$ for 24 h, which intuitively show the intracellular ROS. (D) Optical density of HaCat cells after incubation with EGF (0–80 μg/ml) for 12, 24, 48 and 72 h. (E) IL-6 level and (F) TNF-α level of HaCat cells preincubated with EGF (80 ng/ml) for 1 h before treatment with different preparations for 24 h. Data are expressed as the mean ± SD, $n = 3$, *$P < 0.05$, **$P < 0.01$, ***$P < 0.001$.**

We adopted the $H_2O_2$-induced model to evaluate the antioxidant ability of $TCeO_2$-TRA-FNL. We found that cell viability was 73.57% ± 1.86% when the concentration of $H_2O_2$ reached 750 μM, which was appropriate in the following research (Fig. 4A). Acting as an important antioxidant in the body, the enzyme activity of SOD is always used to evaluate antioxidant capacity [47]. The result shown in Fig. 4B implied that compared with $H_2O_2$-stimulated cells, $TCeO_2$-TRA-FNL could dramatically increase SOD level and was more efficient than free TRA ($P < 0.01$). This was mainly because liposomes promoted better intracellular drug delivery and $TCeO_2$ achieved better clearance of intracellular ROS. It was found that $TCeO_2$ still effectively scavenged ROS despite being encapsulated into liposomes, which was consistent with a previous study [64]. The 2′,7′-dichlorodihydrofluorescein diacetate (DCFH-DA) can be oxidized from a nonfluorescent module to a fluorescent agent, so we use it to detect intracellular ROS [65]. According to the result in Fig. 4C, the green fluorescence intensity increased after treatment with $H_2O_2$. Nevertheless, the green fluorescence intensity decreased after incubation with different preparations, especially $TCeO_2$-TRA-FNL, indicating that the ability of $TCeO_2$-TRA-FNL to scavenge ROS was better than that of the other preparations. According to the SOD and ROS results, we believed that $TCeO_2$-TRA-FNL had superior antioxidant capacity *in vitro*.

Epidermal growth factor (EGF) is involved in cell growth, differentiation, and proliferation [66]. So we utilized EGF to imitate the state of psoriasis. First, we examined the incubation concentration and time of EGF by measuring optical density. As shown in Fig. 4D, optical density was positively correlated with concentration and time. We finally chose to incubate with 80 ng/ml EGF for 24 h as the modeling condition. Then, IL-6 and TNF-α levels were estimated. Fig. 4E and 4F showed that after incubation with $TCeO_2$-TRA-FNL, the two levels decreased compared with that in the EGF treatment group ($P < 0.01$). The results demonstrated that $TCeO_2$-TRA-FNL had good anti-inflammatory capability, possibly because TRA exerted an anti-inflammatory effect. In addition, $TCeO_2$ removed intracellular ROS, which might inhibit some signal pathways to alleviate inflammation[16]. The reason why there was no significant difference between the other groups and the $TCeO_2$-TRA-FNL group might be that the growth state and density of cells were difficult to control completely consistently, although we assigned the same initial cell count to each group.

### 3.6. In vivo *efficiency against psoriasis*

IMQ can serve as an agonist of TLR-7/8 to promote the occurrence of psoriasis [67]. Hence, the ability of $TCeO_2$-TRA-FNL-Gel to alleviate psoriasis was further investigated in an IMQ-induced model [49]. BALB/c mice were randomly divided into seven groups: (1) control group, (2) IMQ group, (3) $TCeO_2$-TRA-FNL-Gel group, (4) $TCeO_2$-FNL-Gel group, (5) $CeO_2$-FNL-Gel group, (6) TRA-FNL-Gel group, and (7) Free-TRA-Gel group (for each group, $n = 5$).

The results of weight changes were shown in Fig. 5A. Obviously, no significant changes were observed during the experiment. The skin compliance study was conducted on the skin of mice to evaluate the safety of gels we prepared [49,50]. We found that the application of Free-TRA-Gel for 7 d could cause skin irritation, which confirmed the skin side effect of TRA. In contrast, other groups didn't observe skin irritation (Fig. 5B). This result confirmed that the skin irritation could be reduced by encapsulating TRA into liposomes. The possible reason was that the liposomes could hydrate the epidermis simply by providing lipids to the stratum corneum [68]. The results demonstrated that $TCeO_2$-TRA-FNL-Gel can increase the safety during application.

Erythema, scaling and skin thickness are prominent features of psoriasis [69]. Hence, we evaluated these indexes in mice during the experiment. Clearly, the mice in the IMQ group had features mentioned above, accompanied by symptoms of redness and swelling and after treatment with different preparations, especially $TCeO_2$-TRA-FNL-Gel, these symptoms were alleviated to varying degrees, with the reduction in scale and skin thickness being the most evident (Fig. 5F). Meanwhile, the scores of erythema and scale and skin thickness of mice in each treatment group were lower (Fig. 5C and 5E). Compared with the Free-TRA-Gel group, the scores of erythema and scale and skin thickness in the $TCeO_2$-TRA-

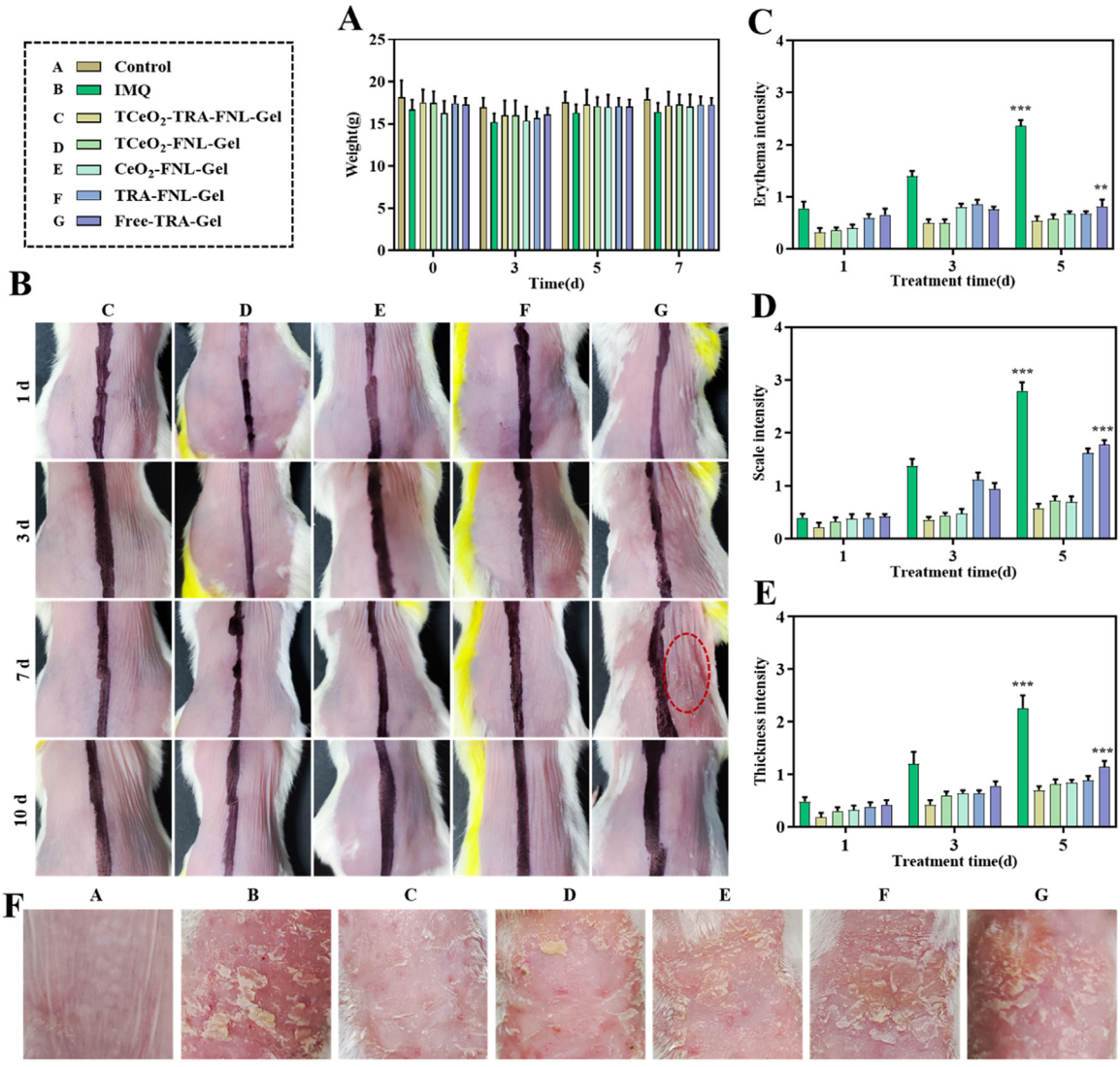


**Fig. 5 – *In vivo* antipsoriasis effect. (A) Weight on Day 0, 3, 5, and 7. (B) Skin irritation result (left: blank Gel, right: different formulations). (C-E) PASI scores of mice. (F) Final images of diseased skin. Data are expressed as the mean ± SD, $n \geq 3$, *$P < 0.05$, **$P < 0.01$, ***$P < 0.001$, compared with the $TCeO_2$-TRA-FNL-Gel group.**

FNL-Gel group were significantly reduced (erythema: $P < 0.01$; scale and skin thickness: $P < 0.001$). The limited effect of Free-TRA-Gel might be attributed to the difficult skin delivery and skin irradiation of TRA. The results proved that $TCeO_2$-TRA-FNL-Gel was beneficial for reducing erythema and scaling and inhibiting skin thickness, indicating that using liposomes to encapsulate TRA could reduce side effects and improve anti-psoriasis effects.

It is widely reported that both IL-6 and TNF-$\alpha$ participate in the pathological process of psoriasis, and they are considered indications for disease severity [70,71]. We used ELISA kits to determine the two levels. From the results in Fig. 6A and 6B, we observed that the two levels were downregulated after treatment with $TCeO_2$-TRA-FNL-Gel, which was significantly different from the IMQ group (IL-6: $P < 0.01$; TNF-$\alpha$: $P < 0.001$). Meanwhile, a similar tendency appeared when compared with the Free-TRA-Gel group (IL-6: $P < 0.001$; TNF-$\alpha$: $P < 0.05$). The results explained that $TCeO_2$-TRA-FNL-Gel had an enormous capacity to relieve inflammation in psoriatic skin.

ROS levels in skin tissue were detected by immunofluorescence. Fig. 6D showed that the ROS level was significantly higher in IMQ group. After incubation with different gels, the red fluorescence intensity decreased. The red fluorescence intensity in the $TCeO_2$-TRA-FNL-Gel group was the lowest, which illustrated that ROS nearly recovered to normal levels. Furthermore, Fig. 6C showed that SOD levels were upregulated after incubation with different preparations. The SOD level of the $TCeO_2$-TRA-FNL-Gel group was higher compared with the IMQ and Free-TRA-Gel groups (IMQ: $P < 0.01$; Free-TRA-Gel: $P < 0.05$). The results above demonstrated that $TCeO_2$-TRA-FNL-Gel could effectively relieve the oxidative stress of skin.

Excessive proliferation of keratinocytes, infiltration of inflammatory cells, and angiogenesis commonly exist in

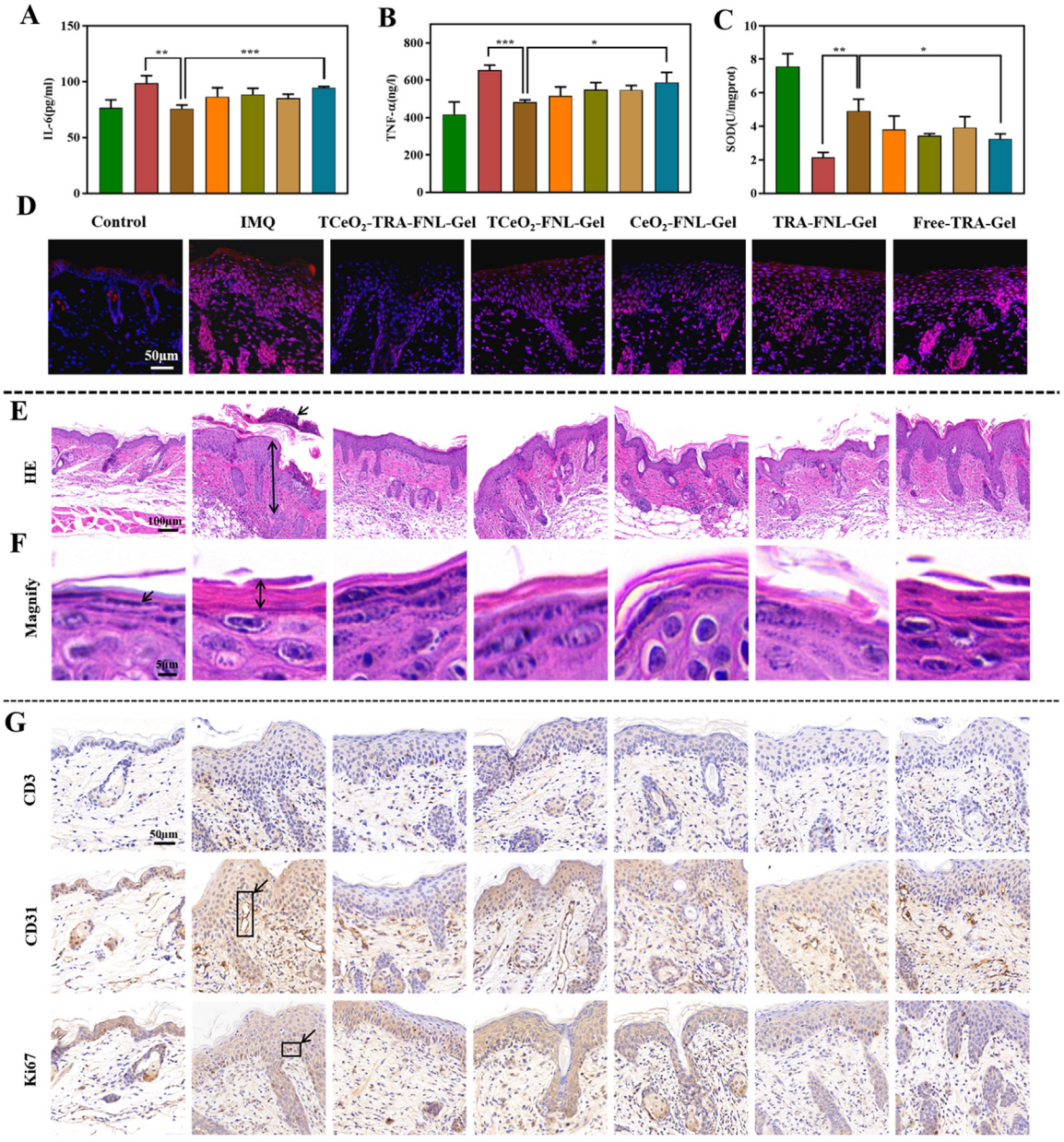


**Fig. 6 – *In vivo* efficiency against psoriasis. (A) IL-6 level and (B) TNF-$\alpha$ level of diseased skin after different treantment. (C) SOD activity of diseased skin after different treantment. (D) Immunofluorescence images of diseased skin (red represents ROS). (E-F) H&E-stained diseased skin with different scale bars. (G) Expression of CD3, CD31 and Ki67. Data are expressed as the mean ± SD, $n = 3$, *P < 0.05, **P < 0.01, ***P < 0.001, compared with the $TCeO_2$-TRA-FNL-Gel group.**

psoriasis [72,73]. They were evaluated by H&E staining and immunohistochemistry.

Skin thickening, elongation of the epidermal crest and Munro microabscess are regarded as the main histopathological features of psoriasis [74]. As shown in Fig. 6E and 6F, we observed similar features in the IMQ group. Furthermore, the stratum corneum thickened and the granular layer disappeared after the application of IMQ. After treatment with Free-TRA-Gel, the thickening of the skin showed little reduction. In contrast, the $TCeO_2$-TRA-FNL-Gel group showed an obvious reduction, suggesting that $TCeO_2$-TRA-FNL-Gel was capable of inhibiting the epidermal thickening of psoriatic skin.

CD3, CD31, and Ki67 are vital markers in psoriatic skin, and they are always used to evaluate the severity of psoriasis [49,75,76]. The results in Fig. 6G suggested that the levels of CD3, CD31, and Ki67 in the IMQ group were noticeably increased. However, the three levels were decreased after treatment and the $TCeO_2$-TRA-FNL-Gel group had the lowest levels. The downregulation of CD3, CD31, and Ki67 might be attributed to the fact that $TCeO_2$-TRA-FNL-Gel relieved inflammation related to excessive proliferation of keratinocytes and angiogenesis.

According to the results mentioned above, we could see that $TCeO_2$-TRA-FNL-Gel had great antipsoriasis capacity *in vivo*, which could be attributed to the high drug retention and deep penetration of the liposome-gel system, thus maximizing the drug effect. Despite the satisfying results we obtained, some limitations in the *in vivo* study were also demonstrated later. The sample size was insufficient in comparison with clinical trials, and individual differences might affect the statistical analysis.

## 4. Conclusion

In summary, a nanotransdermal delivery system composed of TRA and TPP-modified $CeO_2$ nanoparticles, flexible nanoliposomes, and gels ($TCeO_2$-TRA-FNL-Gel) was successfully constructed, and its effect was evaluated. $TCeO_2$-TRA-FNL with an appropriate size can excellently enter the keratinocytes after overcoming obstacles from the stratum corneum. The effect is apparent with the release of TRA and $TCeO_2$. TRA can inhibit the excessive proliferation of keratinocytes, and $TCeO_2$ can target mitochondria to eradicate excessive ROS. The synergistic effect endows the system with satisfying anti-inflammatory and antioxidant capacities. Overall, this nanotransdermal delivery system is a prospective strategy for the treatment of psoriasis. Unfortunately, the insufficient sample size in our study makes it difficult to provide practical guidance for clinical research. In the future, the sample size can be expanded, and other strains of animals can also be used *in vivo* to verify the universality of our system.

## Conflicts of Interest

The authors report no conflicts of interest. The authors alone are responsible for the content and writing of this article.

## Acknowledgments

This research was supported by Zhejiang Provincial Natural Science Foundation of China under Grant No. LYY21H300001, Zhejiang Medical and Health Science and Technology project under Grant No. 2021KY906 and Hangzhou Medical Key Discipline Construction Project under Grant No. [2021]21–39.

## Supplementary materials

Supplementary material associated with this article can be found, in the online version, at doi:10.1016/j.ajps.2023.100846.

REFERENCES

[1] Yan BX, Chen XY, Ye LR, Chen JQ, Zheng M, Man XY. Cutaneous and systemic psoriasis: classifications and classification for the distinction. Front Med Lausanne 2021;8:649408.
[2] Parisi R, Iskandar IYK, Kontopantelis E, Augustin M, Griffiths CEM, Ashcroft DM, et al. National, regional, and worldwide epidemiology of psoriasis: systematic analysis and modelling study. BMJ 2020;369:m1590.
[3] Baylet A, Laclaverie M, Marchand L, Bordes S, Closs-Gonthier B, Delpy L. Immunotherapies in cutaneous pathologies: an overview. Drug Discov Today 2021;26(1):248–55.
[4] Nimbalkar M, Yawalkar M, Mahajan N, Dhoble SJ. Potential of luminescent materials in phototherapy. Photodiagnosis Photodyn Ther 2021;33:102082.
[5] Chen A, Luo Y, Xu J, Guan X, He H, Xuan X, et al. Latest on biomaterial-based therapies for topical treatment of psoriasis. J Mater Chem B 2022;10(37):7397–417.
[6] Brandon A, Mufti A, Gary Sibbald R. Diagnosis and management of cutaneous psoriasis: a review. Adv Skin Wound Care 2019;32(2):58–69.
[7] Biswasroy P, Pradhan D, Kar B, Ghosh G, Rath G. Recent advancement in topical nanocarriers for the treatment of psoriasis. AAPS PharmSciTech 2021;22(5):164.
[8] Baldwin H, Webster G, Stein Gold L, Callender V, Cook-Bolden FE, Guenin E. 50 years of topical retinoids for acne: evolution of treatment. Am J Clin Dermatol 2021;22(3):315–27.
[9] Lu KJ, Wang W, Xu XL, Jin FY, Qi J, Wang XJ, et al. A dual deformable liposomal ointment functionalized with retinoic acid and epidermal growth factor for enhanced burn wound healing therapy. Biomater Sci 2019;7(6):2372–82.
[10] Rodriguez-Amigo B, Hally C, Roig-Yanovsky N, Delcanale P, Abbruzzetti S, Agut M, et al. A double payload complex between hypericin and all-trans retinoic acid in the beta-lactoglobulin protein. Antibiotics 2022;11(2):282 Basel.
[11] Xia L, Li R, Wang Y, Lin Z, Zheng J, Li X, et al. Efficacy, safety, and cost-effectiveness of all-trans retinoic acid/clobetasol propionate compound ointment in the treatment of mild to moderate psoriasis vulgaris: a randomized, single-blind, multicenter clinical trial. Dermatol Ther 2018;31(5):e12632.
[12] Szymanski L, Skopek R, Palusinska M, Schenk T, Stengel S, Lewicki S, et al. Retinoic acid and its derivatives in skin. Cells 2020;9(12):2660.
[13] Wang HM, Wu C, Jiang YY, Wang WM, Jin HZ. Retinol and vitamin A metabolites accumulate through RBP4 and STRA6 changes in a psoriasis murine model. Nutr Metab 2020;17:5 Lond.
[14] Omar SSS, Hadi H. Advancement of all-trans retinoic acid delivery systems in dermatological application. Cosmetics 2022;9(6):140.
[15] Cannavo SP, Riso G, Casciaro M, Di Salvo E, Gangemi S. Oxidative stress involvement in psoriasis: a systematic review. Free Radic. Res. 2019;53(8):829–40.
[16] Xu F, Xu J, Xiong X, Deng Y. Salidroside inhibits MAPK, NF-κB, and STAT3 pathways in psoriasis-associated oxidative stress via SIRT1 activation. Redox Report 2019;24(1):70–4.
[17] Li P, Li Y, Jiang H, Xu Y, Liu X, Che B, et al. Glabridin, an isoflavan from licorice root, ameliorates imiquimod-induced psoriasis-like inflammation of BALB/c mice. Int Immunopharmacol 2018;59:243–51.
[18] Lai R, Xian D, Xiong X, Yang L, Song J, Zhong J. Proanthocyanidins: novel treatment for psoriasis that reduces oxidative stress and modulates Th17 and Treg cells. Redox Report 2018;23(1):130–5.
[19] Frasheri L, Schielein MC, Tizek L, Mikschl P, Biedermann T, Zink A. Great green tea ingredient? A narrative literature review on epigallocatechin gallate and its biophysical properties for topical use in dermatology. Phytother Res 2020;34(9):2170–9.

[20] Bao Q, Hu P, Xu Y, Cheng T, Wei C, Pan L, et al. Simultaneous blood-brain barrier crossing and protection for stroke treatment based on edaravone-loaded ceria nanoparticles. ACS Nano 2018;12(7):6794–805.
[21] Huang Y, Ren J, Qu X. Nanozymes: classification, catalytic mechanisms, activity regulation, and applications. Chem Rev 2019;119(6):4357–412.
[22] Yadav N. Cerium oxide nanostructures: properties, biomedical applications and surface coatings. 3 Biotech 2022;12(5):121.
[23] Choi SW, Kim J. Recent progress in autocatalytic ceria nanoparticles-based translational research on brain diseases. ACS Appl Nano Mater 2020;3(2):1043–62.
[24] Machhi J, Yeapuri P, Markovic M, Patel M, Yan W, Lu Y, et al. Europium-doped cerium oxide nanoparticles for microglial amyloid beta clearance and homeostasis. ACS Chem Neurosci 2022;13(8):1232–44.
[25] Malsin ES, Kamp DW. The mitochondria in lung fibrosis: friend or foe? Transl Res 2018;202:1–23.
[26] Kim SJ, Cheresh P, Jablonski RP, Williams DB, Kamp DW. The role of mitochondrial DNA in mediating alveolar epithelial cell apoptosis and pulmonary fibrosis. Int J Mol Sci 2015;16(9):21486–519.
[27] Therianou A, Vasiadi M, Delivanis DA, Petrakopoulou T, Katsarou-Katsari A, Antoniou C, et al. Mitochondrial dysfunction in affected skin and increased mitochondrial DNA in serum from patients with psoriasis. Exp Dermatol 2019;28(1):72–5.
[28] Zhang Q, Raoof M, Chen Y, Sumi Y, Sursal T, Junger W, et al. Circulating mitochondrial DAMPs cause inflammatory responses to injury. Nature 2010;464(7285):104–7.
[29] Zheng HF, Zhang YN, He JN, Yang Z, Zhang R, Li L, et al. Hydroxychloroquine inhibits macrophage activation and attenuates renal fibrosis after ischemia-reperfusion injury. Front Immunol 2021;12:645100.
[30] Tonello S, Rizzi M, Migliario M, Rocchetti V, Renò F. Low concentrations of neutrophil extracellular traps induce proliferation in human keratinocytes via NF-$\kappa$B activation. J Dermatol Sci 2017;88(1):110–16.
[31] Mann-Nüttel R, Ali S, Petzsch P, Köhrer K, Alferink J, Scheu S. The transcription factor reservoir and chromatin landscape in activated plasmacytoid dendritic cells. BMC Genomic Data 2021;22(1):37.
[32] Huang T, Zhang TY, Jiang XC, Li A, Su YQ, Bian Q, et al. Iron oxide nanoparticles augment the intercellular mitochondrial transfer-mediated therapy. Sci Adv 2021;7(40): eabj0534.
[33] Ullah H, Di Minno A, Santarcangelo C, Khan H, Daglia M. Improvement of oxidative stress and mitochondrial dysfunction by $\beta$-caryophyllene: a focus on the nervous system. Antioxidants 2021;10(4):546.
[34] Van Houten B, Woshner V, Santos JH. Role of mitochondrial DNA in toxic responses to oxidative stress. DNA Repair(Amst) 2006;5(2):145–52.
[35] Zhang J, Yang C, Pan S, Shi M, Li J, Hu H, et al. Eph A10-modified pH-sensitive liposomes loaded with novel triphenylphosphine-docetaxel conjugate possess hierarchical targetability and sufficient antitumor effect both *in vitro* and *in vivo*. Drug Deliv 2018;25(1):723–37.
[36] Cheng X, Feng D, Lv J, Cui X, Wang Y, Wang Q, et al. Application prospects of triphenylphosphine-based mitochondria-targeted cancer therapy. Cancers(Basel) 2023;15(3):666.
[37] Gungor S, Kahraman E. Nanocarriers mediated cutaneous drug delivery. Eur J Pharm Sci 2021;158:105638.
[38] Liu L, Zhao W, Ma Q, Gao Y, Wang W, Zhang X, et al. Functional nano-systems for transdermal drug delivery and skin therapy. Nanoscale Adv 2023;5(6):1527–58.
[39] Zeinali M, Abbaspour-Ravasjani S, Soltanfam T, Paiva-Santos AC, Babaei H, Veiga F, et al. Prevention of UV-induced skin cancer in mice by gamma oryzanol-loaded nanoethosomes. Life Sci. 2021;283:119759.
[40] Claudia Paiva-Santos A, Gama M, Peixoto D, Sousa-Oliveira I, Ferreira-Faria I, Zeinali M, et al. Nanocarrier-based dermopharmaceutical formulations for the topical management of atopic dermatitis. Int J Pharm 2022;618:121656.
[41] Abedi-Gaballu F, Dehghan G, Ghaffari M, Yekta R, Abbaspour-Ravasjani S, Baradaran B, et al. PAMAM dendrimers as efficient drug and gene delivery nanosystems for cancer therapy. Appl Mater Today 2018;12:177–90.
[42] Zeinali M, Abbaspour-Ravasjani S, Ghorbani M, Babazadeh A, Soltanfam T, Santos AC, et al. Nanovehicles for co-delivery of anticancer agents. Drug Discov Today 2020;25(8):1416–30.
[43] Lv X, Wu Z, Qi X. High skin permeation, deposition and whitening activity achieved by xanthan gum string vitamin c flexible liposomes for external application. Int J Pharm 2022;628:122290.
[44] Zhao F, Lu J, Jin X, Wang Z, Sun Y, Gao D, et al. Comparison of response surface methodology and artificial neural network to optimize novel ophthalmic flexible nano-liposomes: characterization, evaluation, *in vivo* pharmacokinetics and molecular dynamics simulation. Colloids Surf B Biointerfaces 2018;172:288–97.
[45] Jiang T, Wang T, Li T, Ma Y, Shen S, He B, et al. Enhanced transdermal drug delivery by transfersome-embedded oligopeptide hydrogel for topical chemotherapy of melanoma. ACS Nano 2018;12(10):9693–701.
[46] Yu T, Moon J, Park J, Park YI, Na HB, Kim BH, et al. Various-shaped uniform $Mn_3O_4$ nanocrystals synthesized at low temperature in air atmosphere. Chem Mater 2009;21(11):2272–9.
[47] Yu H, Jin F, Liu D, Shu G, Wang X, Qi J, et al. ROS-responsive nano-drug delivery system combining mitochondria-targeting ceria nanoparticles with atorvastatin for acute kidney injury. Theranostics 2020;10(5):2342–57.
[48] Qazi TH, Muir VG, Burdick JA. Methods to characterize granular hydrogel rheological properties, porosity, and cell invasion. ACS Biomater Sci Eng 2022;8(4):1427–42.
[49] Wang W, Shu GF, Lu KJ, Xu XL, Sun MC, Qi J, et al. Flexible liposomal gel dual-loaded with all-trans retinoic acid and betamethasone for enhanced therapeutic efficiency of psoriasis. J Nanobiotechnol 2020;18(1):80.
[50] Raza K, Singh B, Lohan S, Sharma G, Negi P, Yachha Y, et al. Nano-lipoidal carriers of tretinoin with enhanced percutaneous absorption, photostability, biocompatibility and anti-psoriatic activity. Int J Pharm 2013;456(1): 65–72.
[51] Pirmohamed T, Dowding JM, Singh S, Wasserman B, Heckert E, Karakoti AS, et al. Nanoceria exhibit redox state-dependent catalase mimetic activity. Chem Commun 2010;46(16): 2736–2738.
[52] Yan X, Tan XY, Li YX, Wang HB, Jin JB, Mao YR, et al. A stepwise targeting curcumin derivative, Ser@TPP@CUR, for acute kidney injury. ACS Med Chem Lett 2022;13(4): 554–559.
[53] Li WQ, Wang Z, Hao S, He H, Wan Y, Zhu C, et al. Mitochondria-targeting polydopamine nanoparticles to deliver doxorubicin for overcoming drug resistance. ACS Appl Mater Interfaces 2017;9(20):16793–802.
[54] Verma D. Particle size of liposomes influences dermal delivery of substances into skin. Int J Pharm 2003;258(1–2):141–51.
[55] Zhang ZJ, Osmalek T, Michniak-Kohn B. Deformable liposomal hydrogel for dermal and transdermal delivery of meloxicam. Int J Nanomed 2020;15:9319–35.

[56] Duangjit S, Opanasopit P, Rojanarata T, Ngawhirunpat T. Characterization and *in vitro* skin permeation of meloxicam-loaded liposomes *versus* transfersomes. J Drug Deliv 2011;2011:418316.
[57] Pan F, Huang CY, Sha CH, Huang K. Long-term synergistic analgesic effect analysis of co-delivery bupivacaine and dexmedetomidine loaded by nano multilayer liposome. Sci Adv Mater 2022;14(12):1791–8.
[58] Zhao Y, Song SL, Wang DD, Liu H, Zhang JM, Li ZH, et al. Nanozyme-reinforced hydrogel as a $H_2O_2$-driven oxygenerator for enhancing prosthetic interface osseointegration in rheumatoid arthritis therapy. Nat Commun 2022;13(1):6758.
[59] Wang N, Yao H, Tao Q, Sun J, Ma H, Wang Y, et al. TPE based aggregation induced emission fluorescent sensors for viscosity of liquid and mechanical properties of hydrogel. Chin Chem Lett 2022;33(1):252–6.
[60] How KN, Yap WH, Lim CLH, Goh BH, Lai ZW. Hyaluronic acid-mediated drug delivery system targeting for inflammatory skin diseases: a mini review. Front Pharmacol 2020;11:1105.
[61] Kwon HJ, Cha MY, Kim D, Kim DK, Soh M, Shin K, et al. Mitochondria-targeting ceria nanoparticles as antioxidants for Alzheimer's disease. ACS Nano 2016;10(2):2860–70.
[62] Tashiro T, Sawada Y. Psoriasis and systemic inflammatory disorders. Int J Mol Sci 2022;23(8):4457.
[63] Dobrica EC, Cozma MA, Gaman MA, Voiculescu VM, Gaman AM. The involvement of oxidative stress in psoriasis: a systematic review. Antioxidants 2022;11(2):282.
[64] Asal R, Bhagat S, Singh S. Development of liposome-based antioxidant nanoconstruct for efficient delivery of PTEN plasmid. Mater Today Proc 2019;10:60–5.
[65] Hua Y, Chang T, Jiang K, Wang J, Cui X, Cheng M, et al. ROS-sensitive calcipotriol nano-micelles prepared by methoxypolyethylene glycol (mPEG)- modified polymer for the treatment of psoriasis. Drug Deliv 2022;29(1):1903–13.
[66] Hu Q, Xu S, Ye C, Jia J, Zhou L, Hu G. Novel pituitary actions of epidermal growth factor: receptor specificity and signal transduction for UTS1, EGR1, and MMP13 regulation by EGF. Int J Mol Sci 2019;20(20):5172.
[67] Van Der Fits L, Mourits S, Voerman JS, Kant M, Boon L, Laman JD, et al. Imiquimod-induced psoriasis-like skin inflammation in mice is mediated via the IL-23/IL-17 axis. J Immunol 2009;182(9):5836–45.
[68] Paudel KS, Milewski M, Swadley CL, Brogden NK, Ghosh P, Stinchcomb AL. Challenges and opportunities in dermal/transdermal delivery. Ther Deliv 2010;1(1):109–31.
[69] Ferreli C, Pinna AL, Pilloni L, Tomasini CF, Rongioletti F. Histopathological aspects of psoriasis and its uncommon variants. G Ital Dermatol Venereol 2018;153(2):173–84.
[70] Xu H, Liu J, Niu M, Song S, Wei L, Chen G, et al. Soluble IL-6R-mediated IL-6 trans-signaling activation contributes to the pathological development of psoriasis. J Mol Med (Berl) 2021;99(7):1009–20.
[71] Choi DH, Hwang HS. Anti-inflammation activity of brazilin in TNF-$\alpha$ induced human psoriasis dermatitis skin model. Appl Biol Chem 2019;46:62.
[72] Rendon A, Schakel K. Psoriasis Pathogenesis and Treatment. Int J Mol Sci 2019;20(6):1475.
[73] Krueger G, Ellis CN. Psoriasis–recent advances in understanding its pathogenesis and treatment. J Am Acad Dermatol 2005;53(1 Suppl 1):S94–100.
[74] Tsai YC, Tsai TF. Overlapping features of psoriasis and atopic dermatitis: from genetics to immunopathogenesis to phenotypes. Int J Mol Sci 2022;23(10):5518.
[75] Guo J, Liu Y, Guo X, Meng Y, Qi C, Zhao J, et al. Depressive-like behaviors in mice with Imiquimod-induced psoriasis. Int Immunopharmacol 2020;89(Pt B):107057.
[76] Li J, Hou H, Zhou L, Wang J, Liang J, Li J, et al. Increased angiogenesis and migration of dermal microvascular endothelial cells from patients with psoriasis. Exp Dermatol 2021;30(7):973–81.